Journal of Materials Chemistry C

ROYAL SOCIETY OF CHEMISTRY

PAPER

View Article Online
View Journal | View Issue

Cite this: J. Mater. Chem. C, 2022, 10, 9356

Control over microphase separation and dielectric properties *via para*-fluoro thiol click reaction†

Gokhan Topcu, *[a] David Reinoso Arenas,[b] Steven Huband,[c] Tony McNally [b] and C. Remzi Becer [a]

Received 1st January 2022,
Accepted 8th June 2022

DOI: 10.1039/d2tc00009a

rsc.li/materials-c

Herein, we have reported a *para*-fluoro thiol click reaction allowing control of the microphase separation and dielectric properties of poly(pentafluorostyrene-*b*-acrylic acid) copolymers. The block copolymer of pentafluorostyrene and acrylic acid was synthesized with high block incompatibility by nitroxide mediated polymerisation. By using a *para*-fluoro thiol reaction, 1-dodecanethiol was precisely clicked to block copolymers in various ratios. The microphase structures formed with cylindrical morphologies with a minimum domain size of 5 nm. The orientation of the acrylic acid cylinders varied from horizontal to vertical as the click ratio was increased. The dielectric constant of the copolymers decreases with increasing click ratio because of the low dielectric constant of the dodecane pendant groups and reaches κ = 2.4 (at 1000 Hz). This study provides insights on one-step control over phase and dielectric properties by using a facile and very effective click reaction strategy for the fabrication of novel polymers for next-generation capacitor films used in directed energy and advanced integrated circuits with smaller feature sizes.

Introduction

The growing microelectronics industry requires the miniaturization of device components from transistors to energy storage devices such as capacitors for high-performance applications. To achieve such miniaturization, photolithography has been utilised for several decades; however, the search for smaller systems has been accompanied by the necessity to develop new techniques to overcome production challenges.[1,2] Self-assembly offers a promising alternative manufacturing method for producing materials with dimensions as low as 10 nm.[3,4]

Block copolymers (BCPs) that can spontaneously self-assemble to form nanostructures in various morphologies present a possible solution to current scaling limitations whilst also being relatively easy to fabricate as thin films with reproducible nanostructure across large areas. The thermodynamic driving force leading to the separation of the two (or more) chemically discrete blocks is the main reason for self-assembly on the nanoscale. The morphology, size, and symmetry of the structure are highly governed by the volume fraction of the blocks, the overall degree of polymerisation, and the incompatibility of the constituent monomers (Flory–Huggins parameter, χ). The most frequently studied BCPs for microelectronics are poly(styrene-*b*-ethylene oxide) and poly(styrene-*b*-methyl methacrylate).[5–7] The smallest lamellar domain spacing for these BCPs has been reported as 16 nm and 17.5 nm full-pitch, respectively.[8,9] To further scale down this limit to below 10 nm domain size, various strategies have been reported based on the use of high-χ blocks. For instance, Jo *et al.* reported the bulk film of trifluoroethyl acrylate containing BCPs with a half-pitch of 5 nm,[10] while Hancox *et al.* suggested the use of a fluorinated long-chain initiator as a first block to synthesize polar poly(acrylic acid) presenting a 3.8 nm half-pitch for lamellar morphology.[11] Moreover, Woo *et al.* reported the use of short methacrylic acid block between PS and PMMA blocks to obtain sub-10 nm domains.[12]

On the other hand, the miniaturization of integrated circuits has resulted in excessive power consumption and signal delays in their interconnections.[13–15] To overcome these limitations, materials that are insulating and possess low dielectric constants, have been studied.[16–21] In addition, these low dielectric materials also have important potential applications in the fields of interlayer dielectrics, semiconductor packaging (*e.g.* chips, modules), and high frequency, low-loss boards.[22,23] Typically, the dielectric constant of polymers can be reduced by the incorporation of fluorine atoms into the structure.[24] Therefore, fluorinated polymers are promising candidates not only for phase separation but also as a component for

[a] Department of Chemistry, University of Warwick, Coventry, CV4 7AL, UK. E-mail: gokhan.topcu@warwick.ac.uk
[b] International Institute for Nanocomposites Manufacturing (IINM), WMG, University of Warwick, Coventry, CV4 7AL, UK
[c] Department of Physics, University of Warwick, Coventry, CV4 7AL, UK

† Electronic supplementary information (ESI) available: Includes ^{1}H NMR spectra and GPC traces for PFTR, and detailed approach for polymerisation kinetics for diblock copolymers. See DOI: https://doi.org/10.1039/d2tc00009a

transistor based electronic applications.[25–28] For instance, 2,3,4,5,6-pentafluorostyrene (PFS) which has a low bulk dielectric constant of κ = 2.0–2.4 has been used to enhance the surface characteristics of dielectric layers.[29,30] PFS can be easily modified because the *para*-fluorine atom moieties tend to undergo nucleophilic aromatic substitutions with various nucleophiles, such as amines,[31] alcohols,[32] and especially thiols.[33,34] The most reactive is found to be the basis of the *para*-fluoro thiol reaction (PFTR).[35] Notably, it makes PFTR a versatile route to obtain functional materials with different morphological and dielectric properties by modifying χ and k.

Herein, we report a controlled synthesis of PFS and acrylic acid diblock copolymers and their substitution in various ratios with 1-dodecane thiol *via* PFTR. The morphology and dielectric properties of the BCPs prepared were investigated for different click ratios. To the best of our knowledge, this is the first report of the microphase separation of PFS having an ultra-small domain size and phase control by simply applying PFTR.

Experimental

Materials

2,3,4,5,6-Pentafluorostyrene (97%, Acros Organics) and *tert*-butyl acrylate (98%, Sigma-Aldrich) were purchased and purified by passing through basic AlOx before usage. BlocBuilder MA (Nitroxide initiator, Arkema), trifluoroacetic acid (>99.5%, Alfa Aesar), triethylamine (TEA, ≥99%, Sigma Aldrich), and 1-dodecanethiol (≥98%, Sigma-Aldrich) were supplied and used as received. All solvents including toluene, acetone, methanol, *N*,*N*′-dimethylformamide (DMF), and dichloromethane (DCM) used were analytical grade.

Synthesis of P(PFS-*b*-AA) BCP

Firstly, P(PFS-*b*-*t*BA) block copolymers were synthesized by using nitroxide-mediated polymerisation. The well-defined diblock structure was obtained in two steps by using the first block as a macroinitiator. For the first block, the initiator (114 mg, ≈0.3 mmol) was dissolved in PFS (2 ml, ≈15 mmol, M/I = 50). The reaction mixture was deoxygenated by nitrogen before the vessel was immersed in an oil bath at 120 °C for 5 hours. The polymer obtained was precipitated from DCM into cold methanol to remove the unreacted monomer.

The PPFS macroinitiator (1.62 g, 0.25 mmol, M_n = 6500 g mol^{-1}) was dissolved in toluene (10 ml) and an aliquot of tBA (1.5 ml, 10 mmol, M/I = 40) was added. The reaction mixture was bubbled with nitrogen and heated for 5 hours at 120 °C. The P(PFS-*b*-*t*BA) was precipitated into cold methanol. The white precipitate was collected and dried overnight under a vacuum at 40 °C.

Substitution of dodecanethiol and deprotection

P(PFS-*b*-*t*BA) (100 mg, 0.51 mmol PFS units) and 1-dodecanethiol (150 μL, 0.6 mmol) were dissolved in 3.5 ml of dry DMF and triethylamine (212 μl, 1.53 mmol) were added to the solution. The mixture was stirred at 60 °C for a certain time (*e.g.* from 15 min to 4 h). The solvent was partially removed to an approximate volume of 1 ml and precipitated into cold methanol. The white precipitates were centrifuged (7800 rpm, 10 min), washed twice with methanol, and then dried in a vacuum oven (yield ≈91%).

The substituted BCPs and trifluoroacetic acid were dissolved in DCM. The deprotection reaction was maintained at room temperature overnight. The polymer mixture was washed with acetone 3 times and, all solvent was removed and dried under vacuum (yield ≈ 87%).

Characterization

Gel-permeation chromatography (GPC) analyses were carried out using an Agilent 1260 infinity system operating in THF with 2% TEA and equipped with refractive index and variable wavelength detectors, 2 PL gel 5 μm mixed-C columns (300 × 7.5 mm), a PL gel 5 mm guard column (50 × 7.5 mm) and an auto-sampler. The instrument was calibrated with linear narrow PMMA standards. All samples were filtered through 0.2 μm PTFE filters before analysis. ^{1}H and ^{19}F NMR analyses were performed on Bruker Avance III HD 300 MHz. Atomic Force Microscopy (AFM) images were recorded on a Bruker Dimension Icon operating Quantitative Nanomechanical (QNM) Force in air mode using a silicon tip and nitride lever (t: 650 nm, l: 115 μm, k: 0.4 N m^{-1}). The characterization of dielectric properties was performed with a Parstat MC 2000 card from Princeton Applied Research. The frequency was swept from 10^0 Hz to 10^6 Hz using a two-point copper electrode with an amplitude of 0.5V RMS. Small-angle X-ray scattering (SAXS) measurements were made using a Xenocs Xeuss 2.0 instrument equipped with a micro-focus Cu_Kα source collimated with Scatterless slits. The scattering was measured using a Pilatus 300k detector with a pixel size of 0.172 mm × 0.172 mm.

Results and discussion

The present work suggests a new and simple synthetic strategy for designing and controlling a sub-10 nm domain BCP based on di-block copolymers of PFS and PAA. Upon clicking dodecane thiol pendant chains, the surface/interfacial energy of the blocks at the bounding surfaces of the BCP film can be manipulated. The synthetic approach for the synthesis of P(PFS-*b*-PAA) and controlled modification *via* PFTR are presented in Fig. 1. The BCP of PFS and *t*BA was synthesised by Nitroxide-mediated polymerisation where bulk polymerisation was performed for the synthesis of the first block and toluene was employed for the latter.

The degrees of polymerisation were calculated to be 31 and 33 for PFS and *t*BA, respectively. Subsequently, BCP was reacted with 1-dodecanethiol in the presence of triethylamine. In the last step, a deprotection reaction of the *tert*-butyl groups was performed by using trifluoroacetic acid. As a result, P(PFS-*b*-PAA) having various amounts of the dodecane pendant chain were obtained. For the synthesis of the PFS homopolymer and BCP, a kinetic study was also performed (Fig. S1, ESI†). The

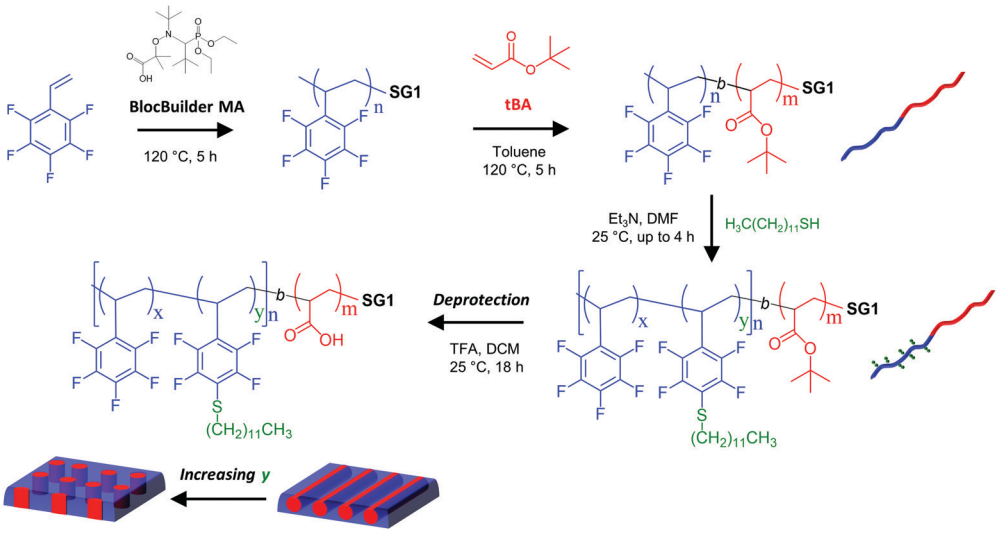

Fig. 1 Schematic representation of overall reaction for synthesis of P(PFS-*b*-AA) following the PFTR of 1-dodecanethiol and cartoon representation of microphase separation in resulting films of final polymers.

monomer conversion was followed by ^{1}H NMR and molecular weight measured by GPC at different reaction times. For each block, monomer conversions were found to be 72% (PFS) and 61% (*t*BA) after 5 h, respectively. The calculated $M_{n,GPC}$ values increased with increasing monomer conversions, which suggests a "living" polymerisation process. Additionally, linear-like regimes were obtained for both block syntheses in the semi-logarithmic kinetic plot, which is consistent with first-order kinetics and the active groups remaining at a constant concentration. On the other hand, the dispersity index ($Đ$) values of the polymers remained narrow between 1.12 and 1.19 even at higher monomer conversions.

Since one of the aims of this work is to control the morphology and domain size by changing the molar fraction (χ also inherently changes), a long hydrocarbon chain was selected, namely 1-dodecanethiol, to reduce the molar fraction of the PAA (f_{PAA}) block in the final compound. The detailed approach for the resulting BCPs by thiol modification is listed in Table 1. The $M_{n,GPC}$ values increased gradually and reached 14 350 g mol^{-1} when the click ratio was 86%. Meanwhile, the f_{PAA} is calculated by the formula presented in ESI† and is found to be decreasing from 0.34 to 0.18. The number of repeating units for the calculation was estimated by GPC. PFTR works well in aprotic polar solvents, therefore, it was performed in DMF. In addition, the process can be readily traced, and the conversion can be calculated using ^{19}F NMR spectroscopy as the *ortho*-, *meta*-, and *para*-fluorine atoms exhibit distinguished and well-separated resonances. The corresponding ^{19}F NMR spectra of the clicked polymers for different reaction times are given in Fig. 2a. The spectrum of *P*1 representing non-clicked P(PFS-*b*-*t*BA) shows three distinct signals at −144, −155, and −162 ppm (labelled as a, c, b), which are assigned to *ortho*, *para*, and *meta* positions, respectively. With regards to pentafluorobenzyl compounds (–CH_2–C_6F_5), the substitution reaction is regioselective, *i.e.*, only *para*-fluorine is substituted. In the PFTR of the P(PFS-*b*-tBA) samples a new signal is observed at −135 ppm that is attributed to new *meta*-fluorine atoms.

The ratio between ^{19}F NMR signals allows for the precise calculation of the click ratio with time, that is, following the kinetics of PFTR for P(PFS-*b*-*t*BA). The reaction was initiated by adding the TEA as a base into the mixture of the polymer and 1-dodecanethiol at room temperature. The reaction was stopped by the precipitation of the clicked polymer in cold methanol at various times for five different batches. The calculated conversions are shown in Fig. 2b. The conversion is around 60% in the first 30 min reaching 86% after 240 min. Similarly, ^{1}H NMR measurements were also performed, and the corresponding spectra show distinct –CH_2 protons at 0.7 ppm due to the long aliphatic chain in 1-dodecanethiol (Fig. S2, ESI†).

Before examining the morphology of the BCPs, the chemical incompatibility between the two blocks was increased *via* the deprotection of the *tert*-butyl pendant group because the resulting acrylic acid block has a more polar nature that can promote distinct phase separation. After an overnight deprotection reaction, ^{1}H NMR spectra indicate a successful reaction (Fig. S3, ESI†) as the signal of methyl protons at 1.4 ppm completely disappears.

It is observed that the deprotection reaction has a dramatic effect on the morphology. While the *tert*-butyl containing

Table 1 Molecular analysis of block copolymers used in this study

	$M_{n,theo}$ (g mol^{-1})	$M_{nGPC,SEC}$ (g mol^{-1})	$Đ$	Click ratio (%)	f_{PFS}	f_{PAA}	f_{C12}
P1	—	10 700	1.19	0	0.57	0.43	—
P2	12 620	12 300	1.15	38	0.46	0.35	0.19
P3	13 680	13 300	1.15	59	0.38	0.29	0.33
P4	14 080	13 500	1.15	67	0.36	0.27	0.37
P5	14 340	13 800	1.14	72	0.34	0.26	0.40
P6	15 050	14 400	1.14	86	0.32	0.24	0.44

[a] $M_{n,theo}$ and $M_{nGPC,SEC}$ are calculated and measured from P(PFS-*b*-*t*BA).

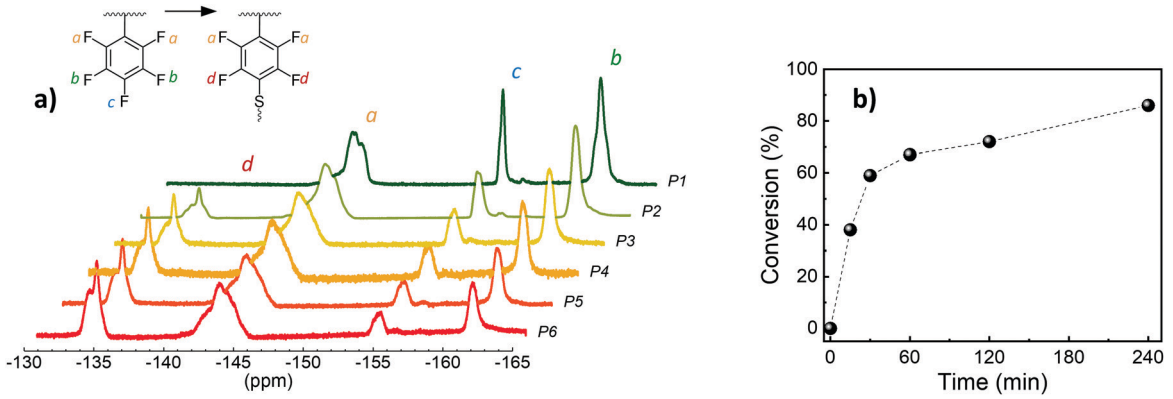

Fig. 2 (a) ^{19}F NMR spectra of P(PFS-*b*-AA) polymers after PFTR for different reaction times. (b) PFTR conversion as a function of time.

sample (*i.e.* before deprotection) shows only an amorphous structure, the deprotected counterpart shows geometric shapes that imply microphase separation (Fig. S4, ESI†). Therefore, to investigate the microphase separation behaviour of the BCPs, a series of films of P(PFS-*b*-AA) with various click ratios and approximately 20 μm thick were prepared by spin coating (1000 rpm, 1 min) acetone solutions (100 mg ml^{-1}) onto meticulously cleaned glass slides and annealing under an acetone-saturated atmosphere in a sealed chamber for 2 days. The morphology of the resulting films was examined by AFM and the corresponding images are presented in Fig. 3a–f. P1 contains the largest volume fraction of the PAA block (f_{PAA}: 0.43) used in this study and shows a phase-separated structure with elongated structures resembling fingerprint shapes. In particular, the morphology of the BCP switches to perpendicular cylindrical with PFTR. P2 and P3 show more ordered cylindrical structures perpendicular to the surface of the substrate, which appear in the light coloured regions, *i.e.*, small mounds, in the AFM images. During the formation of the microphase separation upon solvent annealing, the interaction between solvent and blocks has an inevitable effect on the stacking of polymer chains. Therefore, a change in swelling capability can govern the orientation.[36] Here, the capability of swelling by acetone decreases with the addition of non-polar dodecane chains. Therefore, we assume that this reduction enables the vertically oriented acrylic acid cylinders. Further decrease in f_{PAA} causes a loss in the order of cylinders seen in P4 and P5. However, the light spots are still recognisable confirming the morphology weakly exists. P6 which contains the smallest hydrophilic component shows an amorphous structure while only a small number of cylinders can be identified, presumably since the amount of PAA block in this copolymer is insufficient for phase separation.

The AFM image of P1 suggests the morphology of the BCP may be either lamellar or parallel cylinders. To clarify the geometric shape as a consequence of microphase separation,

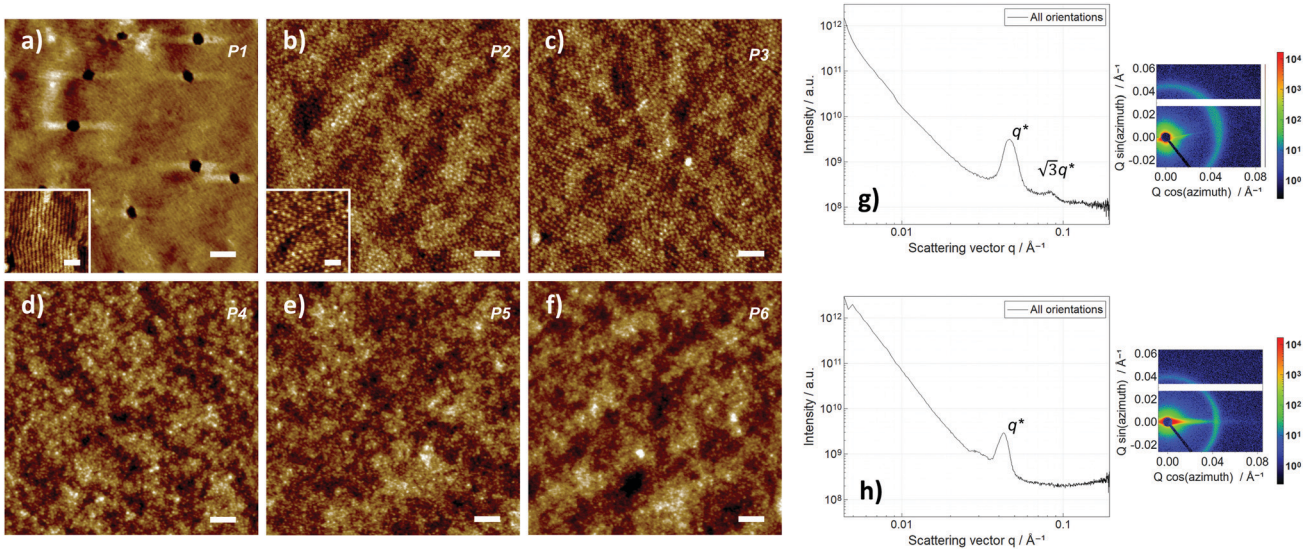

Fig. 3 Height images of P(PFS-*b*-AA) polymers prepared by varying click ratio using the QNM analysis mode of AFM. (a) Parallel cylindrical, (b and c) perpendicular cylindrical, (d and e) weak cylindrical morphologies, and (f) amorphous view of polymers (scale bar: 100 nm, inset scale bar: 50 nm). SAXS response when integrating over all orientations for [1–44] (g) P1 and (h) P2, and 2D SAXS plots measured with the sample surface parallel to the beam.

we performed SAXS measurements on P1 and P2. For these measurements, the polymer films were prepared on Kapton substrates, and a roughly 3 × 3 × 0.3 mm piece of the sample was selected. The samples were mounted such that the X-rays travelled parallel to the surface and in the centre of the beam. This means the horizontal direction of the detector measures the out-of-plane diffraction and the vertical the in-plane diffraction. The measured data for the P1 and P2 samples are shown in Fig. 3g and h. The positions for the peaks in P1 are consistent with the expected positions of q^*, $\sqrt{3}q^*$ and $2q^*$ for hexagonally packed cylinders. Therefore, this confirms that the fingerprint-like structures in the AFM image of P1 are parallel cylinders. In contrast, the SAXS pattern for P2 shows a single diffraction peak. The lack of higher-order peaks may arise from a reduced ordering of the cylinders into a hexagonally packed structure by the click reaction. This is consistent with the decreasing order visible in the AFM images with an increasing click ratio. The *d*-spacing of the q^* peak is given by $2\pi/q$ and corresponds to the average distance from the centre of one cylinder to the next, which were calculated as 13.3 nm and 14.4 nm for P1 and P2 (out of plane), respectively. The 2D plots show in-plane *versus* out-of-plane signals of the polymers for parallel beam alignment. Similarly, the 1D scattering plots show consistent change with the measurement direction (Fig. S5, ESI†). Furthermore, χ parameter for P(PFS-*b*-AA), *i.e.* P1, was also calculated by using the SAXS profile and the Leibler theory.[37,38] The detailed formula and calculation are presented in ESI,† and the χ parameter was found to be 0.246.

The domain size of the polymer samples was also measured from the microscopy images and given as a half-pitch (the distance between boundaries of similar domains, *i.e.*, half of the *d*-spacing calculated by SAXS) in Fig. 4. The gradual colour change refers to morphological alteration due to PFTR. For cylindrical domains, it was assumed that the morphology is in close-packed and ordered structure. Therefore, the size was calculated using a geometrical approach, namely $\sqrt{3}d/2$, where *d* is the diameter of PFS cylinders. The smallest domain size achieved in this work is 5.5 nm for parallel cylinder domains. The domain size consistently increases up to 8.6 nm (P5) as the click ratio is increased. Above that level, no domains are observed in amorphous P6. The PFTR in this work not only governs the χ parameter to change the phase but also increases the molecular mass. It should be noted that the domain size is highly dependent on the molecular mass of the polymer. Therefore, the addition of the hydrocarbon pendant groups using PFTR increases M_n resulting in larger domain sizes. Compared to size data from SAXS, AFM measurements give relatively small domain sizes (domain sizes for P1 d_{AFM}: 5.5 nm and d_{SAXS}: 6.7 nm) since only surface domains are considered, which tend to be more contracted. However, both techniques are consistent and show increasing domain size with PFTR.

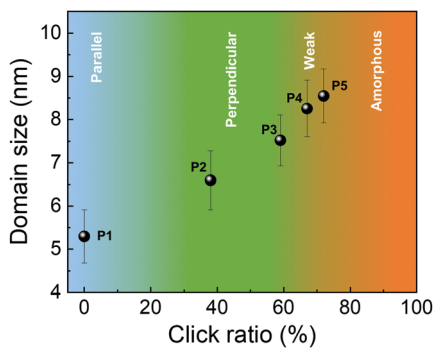

Fig. 4 Domain size (half-pitch) as a function of click ratio for P(PFS-*b*-AA) films with colour map background highlighting the different phases.

As described previously, a low dielectric constant is required to minimize both the signal propagation delay and the dynamic power consumption in on-chip interconnects. The dielectric constant of materials (ε) is dependent on the material structure that defines a total degree of polarisation. In this context, the dielectric properties of P(PFS-*b*-AA) films with all types of structures were measured by Electrical Impedance Spectroscopy (EIS). The BCP samples for electrical characterisation were prepared using multiple coating steps on a round-shaped glass slide with a diameter of 2 cm as polymer films sandwiched between two parallel silver electrode layers (Fig. S6, ESI†). Before coating with a top silver electrode, the samples were annealed under acetone vapour for 2 days. The BCP thickness was kept at 15–20 μm whereas the silver electrode layers were approximately 4 μm. The effect of the click ratio on the dielectric properties of the BCPs was investigated in the frequency range 100 Hz to 100 kHz. Dielectric spectroscopy experiments demonstrated that all P(PFS-*b*-AA) samples have similarly shaped permittivity spectra regardless of morphology in the frequency ranges examined, as shown in Fig. 5a. The morphology independent dielectric properties might have been measured due to both blocks having a continuous phase throughout the film between electrodes. For all samples, the frequency-dependent relative dielectric permittivity values show a constant trend. Comparing P1 and P6, the permittivity shows a slight decrease with an increasing click ratio.

Lichtenecker's rule is an empirical mixing rule that is utilised to predict the dielectric constant of a material having multiple components. The formulation is based on logarithmic dielectric constants and the volume fractions of components,

$$\ln(\kappa_{material}) = f_1 \ln(\kappa_1) + f_2 \ln(\kappa_2) \ldots + f_n \ln(\kappa_n) \quad (1)$$

where κ is the dielectric constant (relative dielectric permittivity) and *f* is the volume fraction. The dielectric constants of the P(PFS-*b*-AA) copolymers were calculated using the reported values for PPFS (κ_{PPFS} = 2.28) and PAA (κ_{PAA} = 5) homopolymers and dodecane (κ_{C12} = 2.01) from the literature.[30,39–42] In Fig. 5b, the predicted dielectric permittivity calculated using the Lichtenecker model is plotted with the experimental dielectric permittivity data at 1000 Hz. The experimental values are in good agreement with the theoretical values, namely, the dielectric permittivity of P(PFS-*b*-AA) copolymers essentially follows the approximation, and the values lie between those of both components. The κ value inherently decreases with increasing click ratio and reaches 2.4 at 86% click ratio (P6) due to the relatively low dielectric constant of the dodecane side chain.

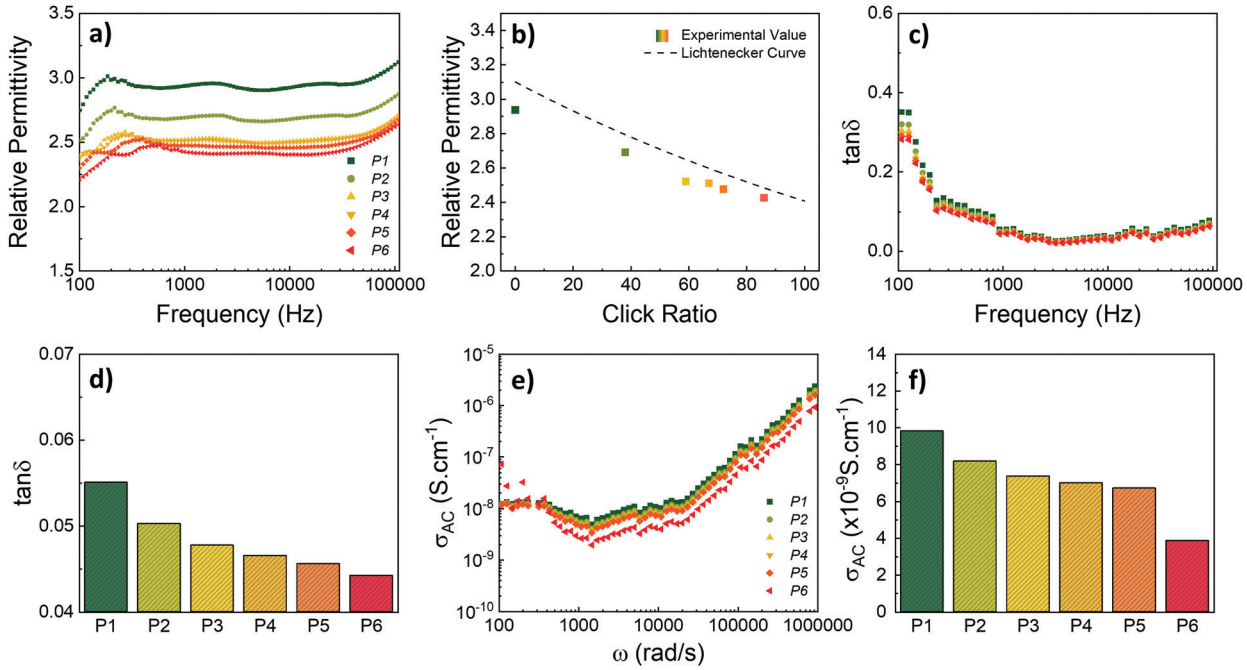

Fig. 5 (a) Relative dielectric permittivity and of P(PFS-*b*-AA) polymers between 100 Hz–100 kHz. (b) Relative permittivity values at 1000 Hz and calculated Lichtenecker curve for same frequency. Dielectric loss ($\tan\delta$) of the polymers (c) between 100–100 KHz and (d) values at 1000 Hz. (e) AC conductivity (σ_{AC}) of the polymers *versus* angular frequency and (f) specific conductivity values at 1000 Hz.

These values indicate that the dielectric permittivity of the BCPs can be modified and lowered without being affected by the morphological change while phase characteristics are also controlled. The dielectric permittivity of these BCPs is comparable to many commercially available polymers.

The dielectric loss factor ($\tan\delta$) is a measure of the energy absorbed in the medium as an electromagnetic wave passes through the material, namely, it quantifies the material's dissipation of electromagnetic energy. In Fig. 5c, $\tan\delta$ of the materials in the frequency range measured is presented and they show similar trends with changing frequency. At lower frequency, the dielectric loss shows a decrease, however, then stabilises above 1000 Hz. This behaviour may be attributed to the relaxation of the polymer films. After stabilisation, the values are sorted as shown in Fig. 5d, and gradually decrease from 0.055 to 0.044 as the click ratio is increased. In general, $\tan\delta$ is known to be influenced by the crystallinity and uniformity of the microstructure as well as the interaction between the nanostructures and the polymer boundary as reported for polymer composites.[27,43] On the contrary, considering this slight decrease is as expected due to the change in the chemical structure of the polymer, no microphase-related effect was observed on dielectric loss. This morphology independent behaviour is due to a stable continuous PFS phase in all-polymer film samples.

The variation of the AC conductivity (σ_{AC}) was measured and the results as a function of angular frequency ($\omega = 2\pi f$) are shown in Fig. 5e. It is observed that, as the click ratio increases, σ_{AC} decreases and the polymer films become more insulating. Typically, σ_{AC} is modelled and described by Jonscher.[44] In most cases, the variation of σ_{AC} as a function of frequency can be classified into separate regions having different characteristics. The conductivity is predominantly due to the AC contribution at high frequencies, which generally increases with increasing frequency. However, it is dominated by DC at low frequency. Therefore, the measurement appears as a plateau and is almost independent of frequency, which is observed in our samples up to $\approx$350 rad s^{-1}. The difference between σ_{AC} of each polymer is more significant in the region above 1000 Hz ($\approx$6280 rad s^{-1}). The σ_{AC} values at this point are presented in Fig. 5f. As predicted from the dielectric constant of the samples, the electrical conductivity values slightly decrease with increasing click ratio and it is seen to be 3.91×10^{-9} S cm^{-1} for P6. Thus, these P(PFS-*b*-AA) block copolymer films are electrically insulating materials.

Conclusions

In summary, we have synthesized block copolymers of pentafluorostyrene and acrylic acid *via* nitroxide-mediated polymerisation resulting in high block incompatibility. By using PFTR, 1-dodecanethiol was clicked to copolymers in various ratios and the self-assembly and dielectric properties of the resultant polymers were studied. Thin films of the synthesized block copolymers were solvent annealed to induce microphase separation, obtaining various morphologies with domain sizes as small as 5.5 nm. EIS measurements of these clicked BCP films indicate that the dielectric permittivity of materials can be lowered by clicking with side groups which have lower relative

permittivity. Therefore, such a modification is a promising route to design a 'metal–insulator' interlayer for next-generation microelectronics since the dielectric constant and morphology can be easily tuned through precise control of the click ratio. By synthesizing potential BCPs consisting of the optimum incompatibility and dielectric properties, it is possible to obtain a catalogue of tailored BCP materials. By using the facile but very effective click reaction strategy, these BCP materials can be used to fabricate nanostructured capacitor films used in directed energy and advanced integrated circuits that require small feature sizes.

Author contributions

G. Topcu – investigation, methodology, writing-original draft and conceptualization D. Reinoso Arenas – EIS measurements, editing manuscript S Huband – SAXS measurement, editing manuscript T. McNally – Review & editing manuscript C. R. Becer – Conceptualization, writing – review and editing, supervision.

Conflicts of interest

There are no conflicts to declare.

Acknowledgements

G. Topcu acknowledges the Scientific and Technological Research Council of Turkey (TUBITAK) for supporting the Postdoctoral Research Fellowship (2219) "No. 1059B191900073".

References

1 C. Sinturel, F. S. Bates and M. A. Hillmyer, *Macro Lett.*, 2015, **4**, 1044–1050.
2 M. Morris, *Microelectron. Eng.*, 2015, **132**, 207–217.
3 C. M. Bates, M. J. Maher, D. W. Janes, C. J. Ellison and C. G. Willson, *Macromolecules*, 2014, **47**, 2–12.
4 M. Luo and T. H. Epps III, *Macromolecules*, 2013, **46**, 7567–7579.
5 S. P. Samant, C. A. Grabowski, K. Kisslinger, K. G. Yager, G. Yuan, S. K. Satija, M. F. Durstock, D. Raghavan and A. Karim, *ACS Appl. Mater. Interfaces*, 2016, **8**, 7966–7976.
6 C. D. Rosa, F. Auriemma, R. D. Girolamo, G. P. Pepe, T. Napolitano and R. Scaldaferri, *Adv. Mater.*, 2010, **22**, 5414–5419.
7 H.-C. Kim, S.-M. Park and W. D. Hinsberg, *Chem. Rev.*, 2010, **110**, 146–177.
8 S. Anastasiadis, T. Russell, S. Satija and C. Majkrzak, *Phys. Rev. Lett.*, 1989, **62**, 1852.
9 T. Ghoshal, C. Ntaras, M. T. Shaw, J. D. Holmes, A. Avgeropoulos and M. A. Morris, *J. Mater. Chem. C*, 2015, **3**, 7216–7227.
10 S. Jo, S. Jeon, T. Jun, C. Park and D. Y. Ryu, *Macromolecules*, 2018, **51**, 7152–7159.
11 E. Hancox, E. Liarou, J. S. Town, G. R. Jones, S. A. Layton, S. Huband, M. J. Greenall, P. D. Topham and D. M. Haddleton, *Polym. Chem.*, 2019, **10**, 6254–6259.
12 S. Woo, S. Jo, D. Y. Ryu, S.-H. Choi, Y. Choe, A. Khan, J. Huh and J. Bang, *ACS Macro Lett.*, 2017, **6**, 1386–1391.
13 J. S. Rathore, L. V. Interrante and G. Dubois, *Adv. Funct. Mater.*, 2008, **18**, 4022–4028.
14 C. Yuan, K. Jin, K. Li, S. Diao, J. Tong and Q. Fang, *Adv. Mater.*, 2013, **25**, 4875–4878.
15 B. Sharma, R. Verma, C. Baur, J. Bykova, J. M. Mabry and D. W. Smith, *J. Mater. Chem. C*, 2013, **1**, 7222–7227.
16 R. D. Miller, *Science*, 1999, **286**, 421–423.
17 Y. Liu, C. Qian, L. Qu, Y. Wu, Y. Zhang, X. Wu, B. Zou, W. Chen, Z. Chen and Z. Chi, *Chem. Mater.*, 2015, **27**, 6543–6549.
18 F. He, Y. Gao, K. Jin, J. Wang, J. Sun and Q. Fang, *ACS Sustainable Chem. Eng.*, 2016, **4**, 4451–4456.
19 W. Volksen, R. D. Miller and G. Dubois, *Chem. Rev.*, 2010, **110**, 56–110.
20 Y. Huang and J. Economy, *Macromolecules*, 2006, **39**, 1850–1853.
21 G. D. Fu, Z. Shang, L. Hong, E. T. Kang and K. G. Neoh, *Adv. Mater.*, 2005, **17**, 2622–2626.
22 X. Lei, M. Qiao, L. Tian, Y. Chen and Q. Zhang, *J. Phys. Chem. C*, 2016, **120**, 2548–2561.
23 M. A. Snyder and M. Tsapatsis, *Angew. Chem., Int. Ed.*, 2007, **46**, 7560–7573.
24 S. Banerjee, G. Maier and M. Burger, *Macromolecules*, 1999, **32**, 4279–4289.
25 K. Kim, T. K. An, J. Kim, Y. J. Jeong, J. Jang, H. Kim, J. Y. Baek, Y.-H. Kim, S. H. Kim and C. E. Park, *Chem. Mater.*, 2014, **26**, 6467–6476.
26 J. Kim, J. Jang, K. Kim, H. Kim, S. H. Kim and C. E. Park, *Adv. Mater.*, 2014, **26**, 7241–7246.
27 R. S. Bharath, T. Chakraborthy, H. Nhalil, B. Masin, K. Ashok, H. Sreemoolanadhan, C. Oommen and S. Elizabeth, *J. Mater. Chem. C*, 2019, **7**, 4484–4496.
28 B. Zhao, C. Zhao, C. Wang and C. B. Park, *J. Mater. Chem. C*, 2018, **6**, 3065–3073.
29 G. Maier, *Prog. Polym. Sci.*, 2001, **26**, 3–65.
30 T. L. Bucholz, S. P. Li and Y.-L. Loo, *J. Mater. Chem.*, 2008, **18**, 530–536.
31 C. Ott, R. Hoogenboom and U. S. Schubert, *Chem. Commun.*, 2008, 3516–3518.
32 P. Zhu, W. Meng and Y. Huang, *RSC Adv.*, 2017, **7**, 3179–3189.
33 C. R. Becer, K. Babiuch, D. Pilz, S. Hornig, T. Heinze, M. Gottschaldt and U. S. Schubert, *Macromolecules*, 2009, **42**, 2387–2394.
34 C. R. Becer, K. Kokado, C. Weber, A. Can, Y. Chujo and U. S. Schubert, *J. Polym. Sci., Part A: Polym. Chem.*, 2010, **48**, 1278–1286.
35 G. Delaittre and L. Barner, *Polym. Chem.*, 2018, **9**, 2679–2684.
36 D. Lee, J. Lee, J. Park and T. Chang, *Macromolecules*, 2020, **53**, 9611–9618.
37 L. Leibler, *Macromolecules*, 1980, **13**, 1602–1617.
38 W. Zha, C. D. Han, D. H. Lee, S. H. Han, J. K. Kim, J. H. Kang and C. Park, *Macromolecules*, 2007, **40**, 2109–2119.

39 L. M. Han, R. B. Timmons, W. W. Lee, Y. Chen and Z. Hu, *J. Appl. Phys.*, 1998, **84**, 439–444.
40 P. C. Sedrez, C. J. N. Sanchez, M. J. da Silva and J. R. Barbosa, *Int. J. Thermophys.*, 2020, **41**, 1–16.
41 S. H. Lim, J. Kim, S.-G. Lee and Y. S. Kim, *Chem. Commun.*, 2010, **46**, 3961–3963.
42 Z. Liu, Z. Yin, S.-C. Chen, S. Dai, J. Huang and Q. Zheng, *Org. Electron.*, 2018, **53**, 205–212.
43 D. F. Miranda, S. Zhang and J. Runt, *Macromolecules*, 2017, **50**, 8083–8096.
44 A. K. Jonscher, *Universal relaxation law: a sequel to Dielectric relaxation in solids*, Chelsea Dielectrics Press, 1996.